

Self-propulsion with speed and orientation fluctuation: Exact computation of moments and dynamical bistabilities in displacement

Amir Shee^{*} and Debasish Chaudhuri[†]

*Institute of Physics, Sachivalaya Marg, Bhubaneswar 751005, India
and Homi Bhabha National Institute, Anushaktinagar, Mumbai 400094, India*

 (Received 31 December 2021; revised 4 April 2022; accepted 2 May 2022; published 26 May 2022)

We consider the influence of active speed fluctuations on the dynamics of a d -dimensional active Brownian particle performing a persistent stochastic motion. The speed fluctuation brings about a dynamical anisotropy even in the absence of shape anisotropy. We use the Laplace transform of the Fokker-Planck equation to obtain exact expressions for time-dependent dynamical moments. Our results agree with direct numerical simulations and show several dynamical crossovers determined by the activity, persistence, and speed fluctuation. The dynamical anisotropy leads to a subdiffusive scaling in the parallel component of displacement fluctuation at intermediate times. The kurtosis remains positive at short times determined by the speed fluctuation, crossing over to a negative minimum at intermediate times governed by the persistence before vanishing asymptotically. The probability distribution of particle displacement obtained from numerical simulations in two dimensions shows two crossovers between compact and extended trajectories via two bimodal distributions at intervening times. While the speed fluctuation dominates the first crossover, the second crossover is controlled by persistence like in the wormlike chain model of semiflexible polymers.

DOI: [10.1103/PhysRevE.105.054148](https://doi.org/10.1103/PhysRevE.105.054148)

I. INTRODUCTION

Active particles self-propel, consuming and dissipating internal or ambient energy [1,2]. They are driven out of equilibrium at the level of individual elements, breaking the detailed balance condition and the equilibrium fluctuation-dissipation relation. Natural examples of active matter span various length scales, including motor proteins, motile cells, bacteria, developing tissues, bird flocks, fish schools, and animal herds [3–8]. Inspired by such biological examples, several artificial active elements were fabricated, e.g., vibrated rods, colloidal swimmers, and asymmetric disks [8,9]. Active colloids can use diffusiophoresis, electrophoresis, and the Marangoni effect to generate self-propulsion [9].

Due to their nonequilibrium nature, active particles show many remarkable properties strikingly different from their equilibrium counterparts. Experimental and theoretical studies gave significant insight into collective motion, flocking, and motility-induced phase separation [8–10]. Even a single active particle can show rich and counterintuitive physical properties. In this context, studies of simple models have been crucial. They displayed several ballistic-diffusive crossovers, non-Boltzmann steady-state, localization away from potential minima, and associated reentrant transition for steady-state properties of trapped particles [11–30].

Fluctuations are inherent to self-propulsion, with its source and nature varying from system to system. For example, ATP hydrolysis in motor proteins or the chemical reaction

in the diffusiophoresis of platinum-gold nanoparticles immersed in hydrogen peroxide is inherently stochastic. The inbuilt structural asymmetry in Janus colloids determines their instantaneous heading direction of motion, which undergoes orientational fluctuations [9]. They are often modeled as active Brownian particles (ABP) performing a continuous-time persistent random walk, assuming a constant active speed [14,31–35]. However, the mechanism of active speed generation itself is stochastic. For example, the speed distribution in the run and tumble motion of *Myxobacteria* is broad [36,37] and, in the pathogenic *E. coli*, it displays a bimodality with peaks corresponding to run and stop [38,39]. This necessitates a description of ABP motion in the presence of speed fluctuations.

In theoretical models, self-propulsion mechanisms can be incorporated in various ways. The energy-depot model is described using a stochastic energy gain and dissipation with a part of dissipated energy leading to self-propulsion [40]. Similarly, coupling internal chemical processes with physical movement leads to a Langevin description of self-propulsion in apolar and polar particles [41,42]. Consideration of a lattice-based model with an internal chemical process generating self-propulsion led to a continuum description similar to the ABP model, apart from the appearance of additional Gaussian noise in active speed [43–45].

In this paper, we consider the impact of such active speed fluctuations on the dynamics of ABPs. The speed fluctuations generate anisotropy to displacement fluctuations [28,29]. We utilize a Laplace transform approach initially developed to understand the properties of the wormlike chain (WLC) model of semiflexible polymers [46] to calculate the exact time dependence of all moments of the ABP in arbitrary dimensions

* amir@iopb.res.in

† debc@iopb.res.in

from the Fokker-Planck equation. Here we summarize our main results.

(1) We present exact computations of several moments of displacement and its components in arbitrary dimensions. At large speed fluctuations, the parallel and perpendicular components of the displacement fluctuation display qualitatively new behavior compared to ABPs with constant speed [21]. They show subdiffusive and ballistic scalings, respectively, in the intermediate time regime.

(2) The exact calculation of displacement kurtosis captures deviations from the Gaussian statistics. Large speed fluctuations keep kurtosis positive over shorter times. At intermediate times the active orientational diffusion leads to negative values of kurtosis before it vanishes asymptotically.

(3) We perform direct numerical simulations in two dimensions to calculate the displacement distribution. With time, it transforms from a distribution with one maximum at the origin to one characterizing extended trajectories to finally return to a Gaussian distribution peaked at the origin. We find two intermediate bimodal distributions among which the first one at a short time is governed by the speed fluctuations. Its presence distinguishes the properties of this system from ABPs with constant speed.

The paper is organized as follows. In Sec. II, we present the model and describe the Laplace transform of the Fokker-Planck equation to derive the general expression for dynamical moments in arbitrary dimensions. In Sec. III, we obtain the mean displacement, mean-squared displacement, and displacement fluctuations. We demonstrate the anisotropy in displacement fluctuations at short times and analyze their crossovers with time. In Sec. IV, we calculate the fourth moment of displacement and kurtosis. Using the kurtosis, we show the deviations of the dynamics from the Gaussian process. In Sec. V we use direct numerical simulations to determine the evolution of the probability distribution function of displacement. Finally, in Sec. VI, we conclude by presenting a summary and outlook.

II. THEORY

A. Model

The dynamics of this active particle in d dimensions is described by its position $\mathbf{r} = (r_1, r_2, \dots, r_d)$ and orientation $\hat{\mathbf{u}} = (u_1, u_2, \dots, u_d)$, which is a unit vector in d dimensions. Let the infinitesimal increments at time t be denoted by $dr_i = r_i(t + dt) - r_i(t)$ and $du_i = u_i(t + dt) - u_i(t)$. Within the Ito convention [47–49], the equation of motion of the ABP with Gaussian speed fluctuation is given by [43]

$$dr_i = (v_0 dt + dB^s) u_i + dB_i^r(t), \quad (1)$$

$$du_i = (\delta_{ij} - u_i u_j) dB_j^r(t) - (d-1) D_r u_i dt, \quad (2)$$

where the translational noise dB^r due to the heat bath follows a Gaussian distribution with its components obeying $\langle dB_i^r \rangle = 0$ and $\langle dB_i^r dB_j^r \rangle = 2D\delta_{ij}dt$. Within a discrete lattice model in Ref. [43], the active displacement was considered to be associated with the release of a chemical potential. In the continuum limit, it led to a speed with deterministic part v_0 and speed fluctuations denoted by an additional Gaussian noise dB^s

obeying $\langle dB^s \rangle = 0$ and $\langle dB^s dB^s \rangle = 2D_v dt$. It is easy to see that dimensionally $D_v = \delta v^2 \tau_v$ with a speed fluctuation δv^2 and an associated relaxation time τ_v . Such a relation can be derived directly considering the mechanism of active speed generation [43, 50–52]. The orientational diffusion of the heading direction is governed by the Gaussian noise dB^r with its components obeying $\langle dB_i^r \rangle = 0$ and $\langle dB_i^r dB_j^r \rangle = 2D_r \delta_{ij} dt$. The first term in Eq. (2) denotes a projection operator for the noise dB^r in the $(d-1)$ -dimensional plane perpendicular to $d\hat{\mathbf{u}}$. The second term ensures the normalization of the unit vector $\hat{\mathbf{u}}^2 = 1 = (\hat{\mathbf{u}} + d\hat{\mathbf{u}})^2$.

It is easy to see from Eq. (1) that the active speed fluctuations lead to anisotropy in displacement fluctuations. The total stochastic force on displacement can be expressed in terms of components along the heading direction $\hat{\mathbf{u}}$ and in the plane perpendicular to it,

$$dB_s u_i + dB_i^r = dB^{\parallel} u_i + dB_j^{\perp} (\delta_{ij} - u_i u_j), \quad (3)$$

where $dB^{\parallel} = dB_s + u_j dB_j^r$ and $dB_j^{\perp} = dB_j^r$. They obey $\langle dB^{\parallel} \rangle = 0$, $\langle dB^{\parallel} dB^{\parallel} \rangle = 2D^{\parallel} dt$ with $D^{\parallel} = (D_v + D)$ and $\langle dB_j^{\perp} \rangle = 0$, $\langle dB_j^{\perp} dB_j^{\perp} \rangle = 2D^{\perp} \delta_{ij} dt$ with $D^{\perp} = D$. This is equivalent to the choice of anisotropic diffusion with $D^{\parallel} > D^{\perp}$ [28, 29, 53]. The anisotropy, in this case, is due to the speed fluctuation $D_v = D^{\parallel} - D^{\perp}$ and not due to shape anisotropy unlike in Refs. [28, 29]. However, the above mapping shows that, expressing D and D_v in terms of D^{\parallel} and D^{\perp} , our work gives a direct method to calculate exact expressions for all the dynamical moments for anisotropic ABP in arbitrary d dimensions. In the following, we present explicit derivations of several such expressions, some of which have been obtained before for anisotropic ABPs in $d = 2, 3$ [28, 29].

It is straightforward to perform direct numerical simulations of Eqs. (1) and (2) using the Euler-Maruyama integration. The units of time and length are set by $\tau_r = 1/D_r$ and $\bar{\ell} = \sqrt{D/D_r}$, respectively. This sets the unit of velocity $\bar{v} = \bar{\ell}/\tau_r = \sqrt{DD_r}$.

B. Fokker-Planck equation and calculation of moments

The probability distribution $P(\mathbf{r}, \hat{\mathbf{u}}, t)$ of the position \mathbf{r} and the active orientation $\hat{\mathbf{u}}$ of the particle follows the Fokker-Planck equation

$$\partial_t P(\mathbf{r}, \hat{\mathbf{u}}, t) = D_v (\hat{\mathbf{u}} \cdot \nabla)^2 P + D_r \nabla_u^2 P + D \nabla^2 P - v_0 \hat{\mathbf{u}} \cdot \nabla P, \quad (4)$$

where ∇ is the d -dimensional Laplacian operator and ∇_u is the Laplacian in the $(d-1)$ dimensional orientation space and can be expressed as $\nabla_u^2 = x^2 \sum_i \partial_{x_i}^2 - [x^2 \partial_x^2 + (d-1)x \partial_x]$ using $u_i = x_i/x$ with $x = |\mathbf{x}|$. Using the Laplace transform $\tilde{P}(\mathbf{r}, \hat{\mathbf{u}}, s) = \int_0^\infty dt e^{-st} P(\mathbf{r}, \hat{\mathbf{u}}, t)$ the Fokker-Planck equation becomes

$$\begin{aligned} & -P(\mathbf{r}, \hat{\mathbf{u}}, 0) + s\tilde{P}(\mathbf{r}, \hat{\mathbf{u}}, s) \\ & = D_v (\hat{\mathbf{u}} \cdot \nabla)^2 \tilde{P} + D_r \nabla_u^2 \tilde{P} + D \nabla^2 \tilde{P} - v_0 \hat{\mathbf{u}} \cdot \nabla \tilde{P}. \end{aligned}$$

The mean of the observable ψ in Laplace space $\langle \psi \rangle_s = \int d\mathbf{r} d\hat{\mathbf{u}} \psi(\mathbf{r}, \hat{\mathbf{u}}) \tilde{P}(\mathbf{r}, \hat{\mathbf{u}}, s)$. Multiplying the above equation by $\psi(\mathbf{r}, \hat{\mathbf{u}})$ and integrating over all possible $(\mathbf{r}, \hat{\mathbf{u}})$

we find

$$-\langle\psi\rangle_0 + s\langle\psi\rangle_s = D_v\langle(\hat{\mathbf{u}} \cdot \nabla)^2\psi\rangle_s + D_r\langle\nabla_u^2\psi\rangle_s + D\langle\nabla^2\psi\rangle_s + v_0\langle\hat{\mathbf{u}} \cdot \nabla\psi\rangle_s, \quad (5)$$

where the initial condition sets $\langle\psi\rangle_0 = \int d\mathbf{r} d\hat{\mathbf{u}} \psi(\mathbf{r}, \hat{\mathbf{u}})P(\mathbf{r}, \hat{\mathbf{u}}, 0)$. Without any loss of generality, we consider the initial condition to follow $P(\mathbf{r}, \hat{\mathbf{u}}, 0) = \delta(\mathbf{r})\delta(\hat{\mathbf{u}} - \hat{\mathbf{u}}_0)$. Equation (5) can be utilized to compute all the moments of any dynamical variable in arbitrary dimensions as a function of time. In the following, we consider moments of displacement and displacement fluctuations characterizing the dynamics.

III. DISPLACEMENT

In Eq. (5) using $\psi = \hat{\mathbf{u}}$ we get $\langle\hat{\mathbf{u}}\rangle_s = \hat{\mathbf{u}}_0/[s + (d-1)D_r]$. The mean displacement can be calculated using $\psi = \mathbf{r}$ in Eq. (5), along with the expression for $\langle\hat{\mathbf{u}}\rangle_s$ to get $\langle\mathbf{r}\rangle_s = v_0\hat{\mathbf{u}}_0/[s + (d-1)D_r]$. Performing an inverse Laplace transform this leads to

$$\langle\mathbf{r}\rangle(t) = \frac{v_0\hat{\mathbf{u}}_0}{(d-1)D_r}(1 - e^{-(d-1)D_r t}). \quad (6)$$

The mean displacement is independent of the speed fluctuation, as dB^s and $\hat{\mathbf{u}}$ are independent stochastic processes and $\langle dB^s \rangle = 0$. This result, thus, is the same as the displacement of ABPs in the absence of speed fluctuations [21].

A. Mean-squared displacement

The mean-squared displacement (MSD) can be calculated using $\psi = \mathbf{r}^2$ in Eq. (5). With initial position at origin, $\langle\mathbf{r}^2\rangle_0 = 0$. It is easy to see that $\langle\nabla_u^2\mathbf{r}^2\rangle_s = 0$, $\langle\hat{\mathbf{u}} \cdot \nabla\mathbf{r}^2\rangle_s = 2\langle\hat{\mathbf{u}} \cdot \mathbf{r}\rangle_s$, $\langle(\hat{\mathbf{u}} \cdot \nabla)^2\mathbf{r}^2\rangle_s = 2\langle 1 \rangle_s$, and $\langle\nabla^2\mathbf{r}^2\rangle_s = 2d\langle 1 \rangle_s$. Note that $\langle 1 \rangle_s = \int d\mathbf{r} d\hat{\mathbf{u}} \hat{P} = \int d\mathbf{r} d\hat{\mathbf{u}} \int_0^\infty dt e^{-st} P = 1/s$ using the normalization $\int d\mathbf{r} d\hat{\mathbf{u}} P = 1$. Thus Eq. (5) leads to

$$s\langle\mathbf{r}^2\rangle_s = 2D_v/s + 2dD/s + 2v_0\langle\hat{\mathbf{u}} \cdot \mathbf{r}\rangle_s.$$

We evaluate $\langle\hat{\mathbf{u}} \cdot \mathbf{r}\rangle_s$ using Eq. (5) again. Utilizing $\nabla_u^2\hat{\mathbf{u}} = -(d-1)\hat{\mathbf{u}}$ and $\langle\hat{\mathbf{u}} \cdot \nabla(\hat{\mathbf{u}} \cdot \mathbf{r})\rangle_s = \langle\hat{\mathbf{u}}^2\rangle_s = 1/s$, we get

$$\langle\hat{\mathbf{u}} \cdot \mathbf{r}\rangle_s = v_0/[s[s + (d-1)D_r]].$$

Using this relation in the expression of $\langle\mathbf{r}^2\rangle_s$ we obtain

$$\langle\mathbf{r}^2\rangle_s = \frac{2D_v}{s^2} + \frac{2dD}{s^2} + \frac{2v_0^2}{s^2[s + (d-1)D_r]}. \quad (7)$$

The inverse Laplace transform gives the MSD

$$\langle\mathbf{r}^2\rangle = 2d\left(D + \frac{v_0^2}{(d-1)dD_r} + \frac{D_v}{d}\right)t - \frac{2v_0^2}{(d-1)^2D_r^2}(1 - e^{-(d-1)D_r t}). \quad (8)$$

The time dependence of MSD is shown in Fig. 1(a). In the long time limit of $D_r t \rightarrow \infty$, it gives a diffusive scaling, $\langle\mathbf{r}^2\rangle = 2d D_{\text{eff}} t$, with the effective diffusion constant

$$D_{\text{eff}} = D + \frac{D_v}{d} + \frac{v_0^2}{(d-1)dD_r}. \quad (9)$$

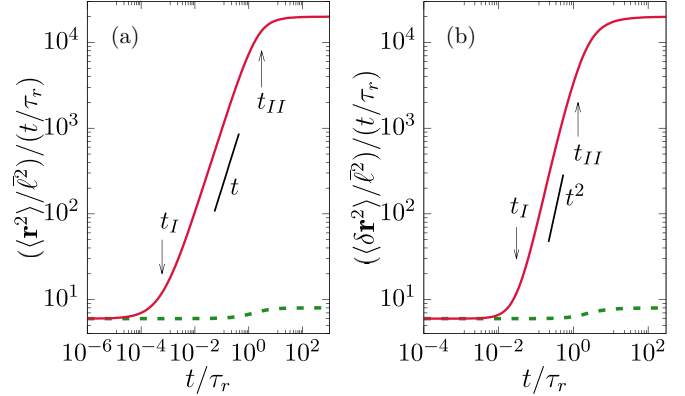


FIG. 1. Time dependence of (a) $\langle\mathbf{r}^2\rangle$ in Eq. (8) and (b) $\langle\delta\mathbf{r}^2\rangle$ in Eq. (10) in $d = 2$ for $Pe = v_0/\bar{v} = 1$ (dashed line) and 100 (solid line), with $\tilde{D}_v = D_v\tau_r/\bar{\ell}^2 = 1$. The crossover times for $Pe = 100$ are (a) $t_I/\tau_r \approx 6 \times 10^{-4}$ and $t_{II}/\tau_r \approx 3$ and (b) $t_I/\tau_r = 0.03$ and $t_{II}/\tau_r \approx 4/3$.

Clearly D_{eff} consists of thermal diffusion D , the contribution from speed fluctuations D_v/d , and the active diffusion due to the persistence of motion $v_0^2/[(d-1)dD_r]$. At $D_v = 0$, the expression for $\langle\mathbf{r}^2\rangle$ agrees with the results for ABPs in the absence of speed fluctuation [21]. Speed fluctuation enhances diffusivity, thereby rendering a mechanism for better spreading which might be utilized, e.g., by pathogenic bacteria in the search of host cells [39].

The effective diffusivity can be reexpressed in terms of the mean translational diffusivity of anisotropic ABP $\bar{D} = [D^{\parallel} + (d-1)D^{\perp}]/d = (D + D_v/d)$ and the active diffusion as

$$D_{\text{eff}} = \bar{D} + \frac{v_0^2}{(d-1)dD_r}.$$

This behavior is similar to ABP with constant speed with the translational diffusion D replaced by the mean diffusivity \bar{D} [21]. Our expression for MSD in Eq. (8) is valid for arbitrary d dimensions. Using $d = 2$, Eq. (8) reduces to the expression for MSD derived for anisotropic ABP in two dimensions [28].

1. Dynamical crossovers

In the small time limit of $t \rightarrow 0$, expanding Eq. (8) around $t = 0$ we get

$$\langle\mathbf{r}^2\rangle = 2d\left(D + \frac{D_v}{d}\right)t + v_0^2 t^2 - \frac{(d-1)}{3}v_0^2 D_r t^3 + O(t^4).$$

Comparing the consecutive terms in the expansion, we can determine the crossover points shown in Fig. 1(a). It predicts the first diffusive $\langle\mathbf{r}^2\rangle \sim t$ to ballistic $\langle\mathbf{r}^2\rangle \sim t^2$ crossover at

$$t_I \approx 2(dD + D_v)/v_0^2,$$

followed by a ballistic to diffusive crossover at

$$t_{II} \approx 3/(d-1)D_r.$$

In Fig. 1(a), these crossover times are identified for parameter values $\tilde{D}_v = D_v\tau_r/\bar{\ell}^2 = 1$ and $Pe = 100$; they are $t_I/\tau_r \approx 6 \times 10^{-4}$ and $t_{II}/\tau_r \approx 3$. Similar crossovers are present at small Pe (Péclet number) as well, but are less pronounced.

B. Displacement fluctuation

Using Eq. (6) and Eq. (8) one can directly obtain the displacement fluctuation $\langle \delta \mathbf{r}^2 \rangle = \langle \mathbf{r}^2 \rangle - \langle \mathbf{r} \rangle^2$ to get

$$\langle \delta \mathbf{r}^2 \rangle = 2dD_{\text{eff}}t - \frac{v_0^2}{(d-1)^2 D_r^2} (3 - 4e^{-(d-1)D_r t} + e^{-2(d-1)D_r t}). \quad (10)$$

This behavior is similar to ABP with constant speed with the translational diffusion D replaced by the increased mean diffusivity \bar{D} , in the expression of D_{eff} [21]. The time dependence of $\langle \delta \mathbf{r}^2 \rangle$ is plotted in Fig. 1(b) at two different Pe values. The plot at large Pe clearly shows a crossover from $\langle \delta \mathbf{r}^2 \rangle \sim t$ to $\langle \delta \mathbf{r}^2 \rangle \sim t^3$ at small t , followed by a crossover back to diffusive $\sim t$ scaling at large t . This can be understood using the expansion

$$\langle \delta \mathbf{r}^2 \rangle = 2(dD + D_v)t + \frac{2}{3}(d-1)v_0^2 D_r t^3 - \frac{1}{2}(d-1)^2 v_0^2 D_r^2 t^4 + O(t^5).$$

$$\langle \delta r_{\parallel}^2 \rangle = 2 \left(D + \frac{D_v}{d} + \frac{v_0^2}{(d-1)dD_r} \right) t + \frac{(d-1)D_v}{d^2 D_r} (1 - e^{-2dD_r t}) + \frac{v_0^2}{D_r^2} \left(\frac{(d-1)e^{-2dD_r t}}{d^2(d+1)} + \frac{8e^{-(d-1)D_r t}}{(d-1)^2(d+1)} - \frac{e^{-2(d-1)D_r t}}{(d-1)^2} - \frac{4d-1}{(d-1)^2 d^2} \right), \quad (11)$$

$$\langle \delta r_{\perp}^2 \rangle = 2(d-1) \left(D + \frac{D_v}{d} + \frac{v_0^2}{(d-1)dD_r} \right) t - \frac{(d-1)D_v}{d^2 D_r} (1 - e^{-2dD_r t}) + \frac{v_0^2}{D_r^2} \left(\frac{4e^{-(d-1)D_r t}}{d^2-1} - \frac{(d-1)e^{-2dD_r t}}{d^2(d+1)} - \frac{3d-1}{d^2(d-1)} \right). \quad (12)$$

In the absence of speed fluctuation $D_v = 0$, the above result reduces to that of usual ABPs with constant active speed [21]. We show comparisons of direct numerical simulations of the model in $d = 2$ with the above-mentioned analytic predictions in Figs. 2 and 3. Remarkably, the parallel component shows a nonmonotonic variation in Fig. 2. The detailed nature of their time dependence is further analyzed in the following.

1. In two dimensions

The expressions simplify in two dimensions, $d = 2$. In the small time limit, expanding the two components around $t = 0$ we obtain

$$\langle \delta r_{\parallel}^2 \rangle_{t \rightarrow 0} = 2(D + D_v)t - 2D_v D_r t^2 + \frac{8}{3}D_v D_r^2 t^3 + \left(\frac{1}{3}v_0^2 - \frac{8}{3}D_v D_r \right) D_r^2 t^4 - \left(\frac{7}{15}v_0^2 - \frac{32}{15}D_v D_r \right) D_r^3 t^5 + O(t^6), \quad (13)$$

$$\langle \delta r_{\perp}^2 \rangle_{t \rightarrow 0} = 2Dt + 2D_v D_r t^2 + \left(\frac{2}{3}v_0^2 - \frac{8}{3}D_v D_r \right) D_r t^3 - \left(\frac{5}{6}v_0^2 - \frac{8}{3}D_v D_r \right) D_r^2 t^4 + O(t^5). \quad (14)$$

It predicts a crossover from diffusive $\langle \delta \mathbf{r}^2 \rangle \sim t$ scaling to $\langle \delta \mathbf{r}^2 \rangle \sim t^3$ scaling at

$$t_I \approx [3(dD + D_v)/(d-1)v_0^2 D_r]^{1/2},$$

followed by another possible crossover back to the diffusive scaling near

$$t_{II} \approx 4/3(d-1)D_r.$$

In Fig. 1(b), the solid line shows the crossovers at $\bar{D}_v = 1$ and $\text{Pe} = 100$. The figure also shows the estimated crossover times $t_I/\tau_r = 0.03$ and $t_{II}/\tau_r = 4/3$.

C. Components of displacement fluctuation

Using the method described above it is straightforward to show that (Appendix A)

The resultant small time limit diffusive scalings are $\langle \delta r_{\parallel}^2 \rangle_{t \rightarrow 0} \approx 2(D + D_v)t$ and $\langle \delta r_{\perp}^2 \rangle_{t \rightarrow 0} \approx 2Dt$. Moreover, the above expansions can be used to identify the observed crossovers. Before analyzing them, we note that the components of displacement fluctuation return to diffusive scaling asymptotically

$$\langle \delta r_{\parallel}^2 \rangle_{t \rightarrow \infty} = \frac{1}{(d-1)} \langle \delta r_{\perp}^2 \rangle_{t \rightarrow \infty} = 2 \left(D + \frac{D_v}{2} + \frac{v_0^2}{2D_r} \right) t. \quad (15)$$

The expressions of differences between these two limits

$$\langle \delta r_{\parallel}^2 \rangle_{t \rightarrow \infty} - \langle \delta r_{\parallel}^2 \rangle_{t \rightarrow 0} = \left(\frac{v_0^2}{D_r} - D_v \right) t, \quad (16)$$

$$\langle \delta r_{\perp}^2 \rangle_{t \rightarrow \infty} - \langle \delta r_{\perp}^2 \rangle_{t \rightarrow 0} = \left(\frac{v_0^2}{D_r} + D_v \right) t$$

are useful for understanding their time dependence. Clearly, $\langle \delta r_{\parallel}^2 \rangle/t$ will reduce (increase) with time for $v_0^2 < D_v D_r$ ($v_0^2 > D_v D_r$). Remarkably, in the absence of speed fluctuation, $D_v = 0$, the possibility of reduction in $\langle \delta r_{\parallel}^2 \rangle/t$ disappears, and such subdiffusive fluctuations are not seen in ABPs with constant active speed [21]. As a result, observation of this measure can be used to distinguish the impact of speed fluctuations in ABP

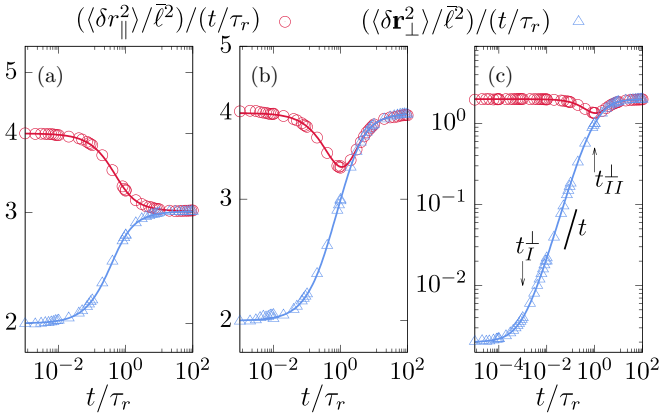


FIG. 2. Components of displacement fluctuation in two dimensions for low activity $\text{Pe}^2 \leq \bar{D}_v$ with $\text{Pe} = v_0 \tau_r / \bar{\ell}$ and $\bar{D}_v = D_v \tau_r / \bar{\ell}^2$. Points denote simulation results and lines depict analytical predictions. The components of displacement fluctuations $\langle \delta r_{\parallel}^2 \rangle$ (\circ , red) and $\langle \delta r_{\perp}^2 \rangle$ (Δ , blue) correspond to Eq. (11) and Eq. (12), respectively. The parameter values used are (a) $\bar{D}_v = 1$ and $\text{Pe} = 0.1$, (b) $\bar{D}_v = 1$ and $\text{Pe} = 1$, and (c) $\bar{D}_v = 10^3$ and $\text{Pe} = 31.62$. The crossover times in (c) are $t_I^{\perp} / \tau_r = 10^{-3}$ and $t_{II}^{\perp} / \tau_r = 1$. The parallel component shows subdiffusive behavior at intermediate time scales as the condition $\text{Pe}^2 \leq \bar{D}_v$ is satisfied.

trajectories obtained from experiments. In contrast, $\langle \delta r_{\perp}^2 \rangle / t$ increases from short time diffusive to asymptotic diffusive behavior, irrespective of the value of active speed.

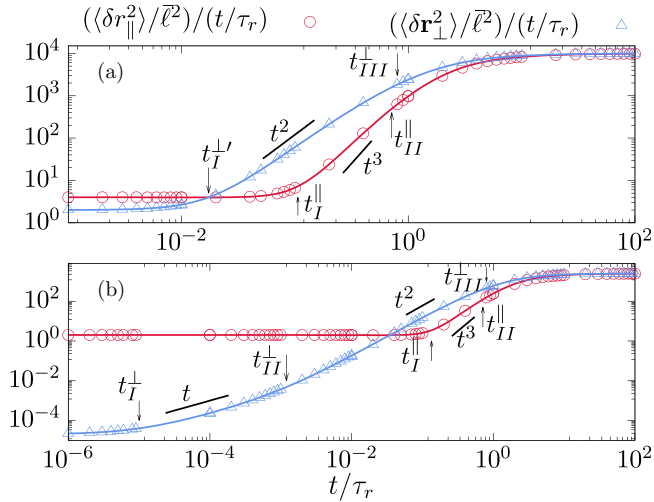


FIG. 3. Components of displacement fluctuation in $d = 2$ for high activity $\text{Pe}^2 > \bar{D}_v$ with $\text{Pe} = v_0 \tau_r / \bar{\ell}$ and $\bar{D}_v = D_v \tau_r / \bar{\ell}^2$. The points denote numerical simulations and the lines denote analytic expressions. The parallel (\circ , red) and perpendicular (Δ , blue) components of displacement fluctuation correspond to Eq. (11) and Eq. (12), respectively. The parameter values used are (a) $\bar{D}_v = 1$ and $\text{Pe} = 10^2$ and (b) $\bar{D}_v = 10^5$ and $\text{Pe} = 1.58 \times 10^4$. In (a), the crossover times are denoted by $t_I^{\parallel} / \tau_r = 0.11$, $t_{II}^{\parallel} / \tau_r = 0.71$, $t_I^{\perp} / \tau_r = 1.7 \times 10^{-2}$, and $t_{III}^{\perp} / \tau_r = 0.8$. In (b), the crossover times are denoted by $t_I^{\parallel} / \tau_r = 0.13$, $t_{II}^{\parallel} / \tau_r = 0.71$, $t_I^{\perp} / \tau_r = 10^{-5}$, $t_{II}^{\perp} / \tau_r = 1.2 \times 10^{-3}$, and $t_{III}^{\perp} / \tau_r = 0.8$.

2. Strong speed fluctuation: $v_0^2 \leq D_v D_r$

In Fig. 2(a), the parallel component shows diffusive–subdiffusive–diffusive crossovers. In Figs. 2(b) and 2(c), $\langle \delta r_{\parallel}^2 \rangle$ shows diffusive–subdiffusive–superballistic–diffusive crossovers. The crossover points can be estimated by comparing the various t scaling in the right hand side of Eq. (13). The first subdiffusive crossover appears at $t_I D_r = (D + D_v) / D_v$. The following superballistic crossover point to $\langle \delta r_{\parallel}^2 \rangle \sim t^3$ is at $t_{II} D_r = 1$. The final diffusive crossover appears at $t_{III} = 8D_v / (8D_v D_r - v_0^2)$.

In the perpendicular component, the crossovers $\langle \delta r_{\perp}^2 \rangle \sim t$ to $\langle \delta r_{\perp}^2 \rangle \sim t^2$ appear at

$$t_I^{\perp} D_r = D / D_v.$$

It is followed by a crossover back to $\langle \delta r_{\perp}^2 \rangle \sim t$ at

$$t_{II}^{\perp} D_r \approx [3D_v D_r / (v_0^2 - 4D_v D_r)]$$

if $v_0^2 < 4D_v D_r$. These crossovers are identified in Fig. 2(c), where with $\bar{D}_v = 10^3$ and $\text{Pe} = 31.62$ the condition $\text{Pe}^2 < 4\bar{D}_v$ holds. The crossover times are $t_I^{\perp} / \tau_r = 10^{-3}$ and $t_{II}^{\perp} / \tau_r = 1$.

The presence of subdiffusive scaling in the parallel component of displacement fluctuations in the intermediate time regime is a characteristic of strong speed fluctuations. It can be measured from direct video microscopy of candidate active Brownian particles. Our predictions can be directly tested against such experiments.

3. Weak speed fluctuation: $v_0^2 > D_v D_r$

In this limit the final diffusivity in $\langle \delta r_{\parallel}^2 \rangle$ is larger than the short time diffusivity. In Fig. 3, we show the crossovers $\langle \delta r_{\parallel}^2 \rangle \sim t$ to $\sim t^4$ and finally to $\sim t$. The crossover times in Fig. 3(a) for $\bar{D}_v = 1$ and $\text{Pe} = 10^2$ are $t_I^{\parallel} / \tau_r \approx 0.11$ and $t_{II}^{\parallel} / \tau_r \approx 0.71$. Similarly, the crossover times in Fig. 3(b) for $\bar{D}_v = 10^5$ and $\text{Pe} = 1.58 \times 10^4$ are $t_I^{\parallel} / \tau_r \approx 0.13$ and $t_{II}^{\parallel} / \tau_r \approx 0.71$.

The crossovers $\langle \delta r_{\perp}^2 \rangle \sim t$ to $\sim t^3$ and finally to $\sim t$ are shown in Fig. 3(a) for $\bar{D}_v = 1$ and $\text{Pe} = 10^2$. The crossover times identified in the figure are $t_I^{\perp} / \tau_r = 1.7 \times 10^{-2}$ and $t_{III}^{\perp} / \tau_r = 0.8$. Another scenario in Fig. 3(b) at $\bar{D}_v = 10^5$ and $\text{Pe} = 1.58 \times 10^4$. The identified crossover times are $t_I^{\perp} / \tau_r = 1 / \bar{D}_v = 10^{-5}$, $t_{II}^{\perp} / \tau_r \approx 1.2 \times 10^{-3}$, and $t_{III}^{\perp} \equiv t_{III}^{\perp} / \tau_r \approx 0.8$. The explicit calculations for the expressions of these crossover times are shown in Appendix C.

IV. FOURTH MOMENT AND KURTOSIS

In this section we obtain the fourth moment of displacement $\langle \mathbf{r}^4 \rangle$ and hence the kurtosis [21,28–30,54] to quantify the deviations from possible Gaussian behavior.

The fourth moment of displacement is given by (Appendix B)

$$\begin{aligned}
\langle \mathbf{r}^4(t) \rangle = & 4[D_v + (d+2)D](D_v + dD)t^2 + 16D_v(D_v + D) \left[\frac{t}{2dD_r} - \frac{1}{(2dD_r)^2} (1 - e^{-2dD_r t}) \right] \\
& + 32D_v(D_v + dD)D_r \left[\frac{t^2}{4dD_r} - \frac{t}{(2dD_r)^2} + \frac{1}{(2dD_r)^3} (1 - e^{-2dD_r t}) \right] \\
& + 8D_v v_0^2 \left[\frac{t^2}{(d-1)D_r} + \frac{t}{(d-1)^2 D_r^2} + \frac{3t e^{-(d-1)D_r t}}{(d-1)^2 D_r^2} - \frac{4}{(d-1)^3 D_r^3} (1 - e^{-(d-1)D_r t}) \right] \\
& + 32D_v v_0^2 \left[\frac{t^2}{2(d-1)dD_r} + \frac{(d^2 - 4d + 1)t}{2(d-1)^2 d^2 D_r^2} + \frac{-3d^3 + 11d^2 - 5d + 1}{4(d-1)^3 d^3 D_r^3} + \frac{(d-3)e^{-(d-1)D_r t}}{(d-1)^3 (d+1)D_r^3} - \frac{(d-1)e^{-2dD_r t}}{4d^3 (d+1)D_r^3} \right] \\
& - \frac{8(d^2 v_0^4 + 10d v_0^4 + 25v_0^4)e^{-(d-1)D_r t}}{(d-1)^4 (d+1)^2 D_r^4} + \frac{4(d^3 v_0^4 + 23d^2 v_0^4 - 7d v_0^4 + v_0^4)}{(d-1)^4 d^3 D_r^4} \\
& + \frac{8t e^{-(d-1)D_r t} (d^3 DD_r v_0^2 + 2d^2 DD_r v_0^2 - d DD_r v_0^2 + d v_0^4 - 2DD_r v_0^2 - 7v_0^4)}{(d-1)^3 (d+1)D_r^3} \\
& + \frac{4t^2 (d^5 D^2 D_r^2 - 3d^3 D^2 D_r^2 + 2d^3 DD_r v_0^2 + 2d^2 D^2 D_r^2 + 2d^2 DD_r v_0^2 - 4d DD_r v_0^2 + d v_0^4 + 2v_0^4)}{(d-1)^2 d D_r^2} \\
& - \frac{8t (d^4 DD_r v_0^2 + d^3 DD_r v_0^2 - 2d^2 DD_r v_0^2 + d^2 v_0^4 + 6d v_0^4 - v_0^4)}{(d-1)^3 d^2 D_r^3}. \tag{17}
\end{aligned}$$

In terms of D^\parallel and D^\perp , the above expression corresponds to anisotropic ABP. Using $d = 2$, it reduces to the result for anisotropic ABP in two dimensions [28].

For $D_v = 0$ Eq. (17) agrees with the fourth moment of the usual ABPs obtained in Ref. [21]. The fourth moment of a general Gaussian process obeys

$$\mu_4 = \langle \mathbf{r}^2 \rangle^2 + \frac{2}{d} (\langle \mathbf{r}^2 \rangle^2 - \langle \mathbf{r}^4 \rangle). \tag{18}$$

Using the expression of $\langle \mathbf{r}^4 \rangle(t)$, the kurtosis in d dimensions is defined as

$$\mathcal{K} = \frac{\langle \mathbf{r}^4 \rangle}{\mu_4} - 1. \tag{19}$$

In Fig. 4(a) we show the comparison between analytic expression (lines) and numerical simulation results (points) in $d = 2$ dimensions for $\langle \mathbf{r}^4 \rangle$. Figure 4(b) shows the time dependence of kurtosis.

A. Crossovers in mean-quartic displacement

To analyze the crossovers in $\langle \mathbf{r}^4 \rangle$ in $d = 2$, we expand the analytical expression in Eq. (17) around $t = 0$ to obtain

$$\begin{aligned}
\langle \mathbf{r}^4(t) \rangle = & (12D_v^2 + 32D_v D + 32D^2)t^2 \\
& + \left[4(3D_v + 4D)v_0^2 - \frac{16}{3}D_v^2 D_r \right] t^3 \\
& + \left(v_0^4 + \frac{16D_v^2 D_r^2}{3} - \frac{16}{3}DD_r v_0^2 - \frac{20}{3}D_v D_r v_0^2 \right) t^4 \\
& - \left(\frac{2}{3}v_0^4 D_r + \frac{64D_v^2 D_r^3}{15} - \frac{4DD_r^2 v_0^2}{3} - \frac{11D_v D_r^2 v_0^2}{3} \right) t^5 \\
& + O(t^6). \tag{20}
\end{aligned}$$

This gives the expression in the short time limit

$$\langle \mathbf{r}^4 \rangle_{t \rightarrow 0} = (12D_v^2 + 32D_v D + 32D^2)t^2. \tag{21}$$

In the long time limit, Eq. (17) for $d = 2$ gives

$$\langle \mathbf{r}^4(t) \rangle_{t \rightarrow \infty} \approx 8 \left[(D_v + 2D)^2 + \frac{2D_v v_0^2}{D_r} \right] t^2. \tag{22}$$

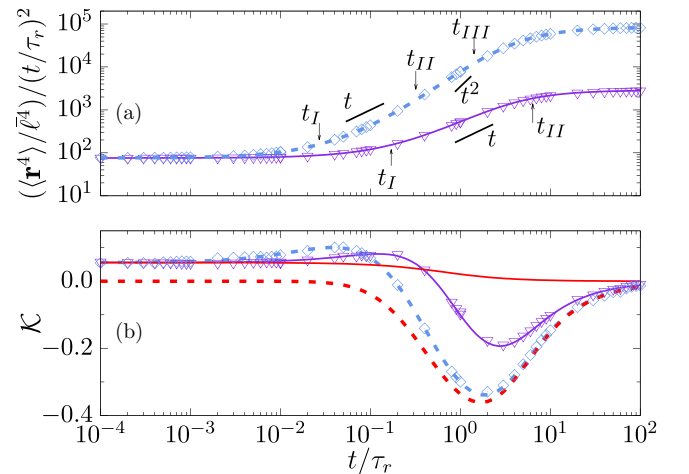


FIG. 4. (a) Fourth moment and (b) kurtosis of displacement as a function of time in $d = 2$. (a) The points denote simulation results and the lines are plots of Eq. (17). The speed fluctuation is set at $\tilde{D}_v = 1$. For $Pe = v_0 \tau_r / \bar{\ell} = 4$ (∇) two crossovers are identified at $t_I / \tau_r \approx 0.17$ and $t_{II} / \tau_r \approx 6.38$. The plot for $Pe = 10$ (\diamond) shows three crossovers at $t_I / \tau_r \approx 0.027$, $t_{II} / \tau_r \approx 0.32$, and $t_{III} / \tau_r \approx 1.42$. (b) Plot of kurtosis \mathcal{K} as a function of time at $Pe = 4$ (∇ , solid line) and $Pe = 10$ (\diamond , dashed line) with $\tilde{D}_v = 1$. The red solid (dashed) line corresponds to $\tilde{D}_v = 1$ (0) and $Pe = 0$ (10). The points denote simulation results and the lines plot Eq. (19).

The difference between the small and long time fourth order moments gives

$$\langle \mathbf{r}^4 \rangle_{t \rightarrow \infty} - \langle \mathbf{r}^4 \rangle_{t \rightarrow 0} \approx \frac{4D_v}{D_r} (4v_0^2 - D_v D_r) t^2, \quad (23)$$

which arises due to the active speed fluctuation. Whether $\langle \mathbf{r}^4 \rangle$ will eventually increase or decrease with time depends on if speed fluctuation is small $4v_0^2 > D_v D_r$ ($\text{Pe}^2 > \tilde{D}_v/4$) or large $4v_0^2 < D_v D_r$ ($\text{Pe}^2 < \tilde{D}_v/4$). The parameter values in Fig. 4(a) obey the condition $\text{Pe}^2 > \tilde{D}_v/4$ and thus show increase in $\langle \mathbf{r}^4 \rangle$ with time. The behavior of kurtosis is qualitatively similar to the anisotropic active Brownian particle [28].

The nature of the crossovers in $\langle \mathbf{r}^4(t) \rangle$ can be analyzed using the expansion in Eq. (20). The solid line in Fig. 4(a) corresponding to $\tilde{D}_v = 1$ and $\text{Pe} = 4$ shows $\langle \mathbf{r}^4(t) \rangle \sim t^2$ to $\sim t^3$ crossover at

$$t_I/\tau_r = 3[3\tilde{D}_v^2 + 8(1 + \tilde{D}_v)]/[3(3\tilde{D}_v + 4)\text{Pe}^2 - 4\tilde{D}_v^2] \approx 0.17,$$

followed by a crossover back to $\sim t^2$ at

$$t_{II}/\tau_r = 4[3(3\tilde{D}_v + 4)\text{Pe}^2 - 4\tilde{D}_v^2]/[3\text{Pe}^4 + 16\tilde{D}_v^2 - 4(4 + 5\tilde{D}_v)\text{Pe}^2] \approx 6.38. \quad (24)$$

The dashed line in Fig. 4(a) corresponding to $\tilde{D}_v = 1$ and $\text{Pe} = 10$ shows the first crossover from $\langle \mathbf{r}^4(t) \rangle \sim t^2$ to $\sim t^3$ at $t_I/\tau_r \approx 0.027$. The second crossover from $\langle \mathbf{r}^4(t) \rangle \sim t^3$ to $\sim t^4$ appears at $t_{II}/\tau_r \approx 0.32$. The final crossover $\langle \mathbf{r}^4(t) \rangle \sim t^4$ to $\sim t^2$ appears at

$$t_{III}/\tau_r = 5[3\text{Pe}^4 + 16\tilde{D}_v^2 - 4(4 + 5\tilde{D}_v)\text{Pe}^2]\tilde{D}_v/[10\text{Pe}^4 + 64 - 5(4 + 11\tilde{D}_v)\text{Pe}^2] \approx 1.42. \quad (25)$$

B. Kurtosis

We show the evolution of kurtosis in Fig. 4(b). Their behavior depends on the competition between persistence v_0^2/D_r and speed fluctuations D_v given by the ratio of Pe^2 and \tilde{D}_v . For finite values of Pe^2 and \tilde{D}_v , it remains positive in the short time regime governed by speed fluctuation. Eventually, the kurtosis shows an intermediate time deviation to negative values, controlled by the orientational fluctuations, before asymptotically vanishing corresponding to a long-time Gaussian limit. In Fig. 4(b), the points denote simulation results and the lines through them plot Eq. (19). We further compare them with the behavior of kurtosis in the (two) limits of finite (vanishing) Pe^2 and vanishing (finite) \tilde{D}_v . At vanishing \tilde{D}_v , our model reduces to traditional ABPs with constant active speed and, as a result, reproduces the known behavior of kurtosis of that model [21]. On the other hand, at vanishing Pe^2 , the behavior of kurtosis is completely dominated by speed fluctuations. It remains positive until vanishing asymptotically at the long time limit. Similar behavior was observed for anisotropic ABPs in two dimensions [28]. As we have mentioned before, due to the direct mapping of our model to anisotropic ABPs, our d -dimensional calculation for kurtosis replacing $D = D^\perp$ and $D_v = D^\parallel - D^\perp$ gives the kurtosis for anisotropic ABPs in arbitrary d dimensions.

In Fig. 5(a), we show a kymograph of kurtosis describing its time evolution at different Pe , keeping the speed fluctuation $\tilde{D}_v = 1$ fixed. The amount of negative deviation of \mathcal{K}

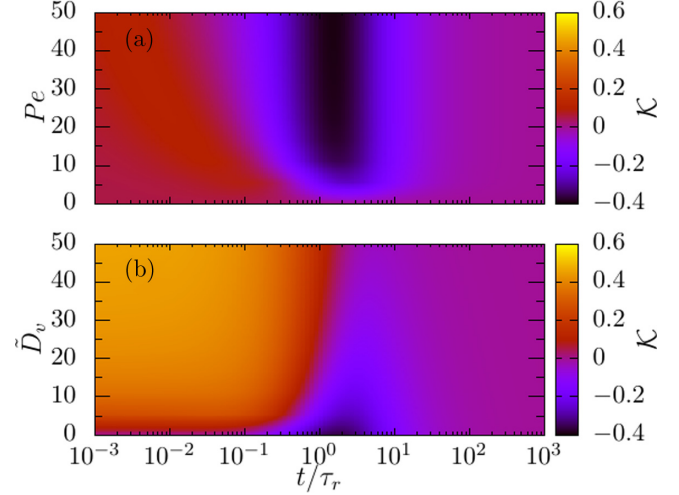


FIG. 5. Deviation from Gaussian nature: kymographs of the kurtosis \mathcal{K} as a function of time t/τ_r of the two-dimensional ABP for different Pe at $\tilde{D}_v = 1$ (a) and for different \tilde{D}_v at $\text{Pe} = 10$ (b).

at intermediate times increases with Pe to eventually saturate at $\mathcal{K} \approx -0.4$. At larger Pe , the deviations towards negative kurtosis appear earlier. At longer times, \mathcal{K} vanishes asymptotically. Figure 5(b) shows the kymograph of \mathcal{K} describing its time evolution at different speed fluctuations \tilde{D}_v for a fixed $\text{Pe} = 10$. At short times \mathcal{K} remains positive, showing increased positive deviations in the presence of larger speed fluctuation \tilde{D}_v . As before, \mathcal{K} shows deviations to negative values at intermediate times before vanishing asymptotically. However, the onset of negative deviations of kurtosis requires a longer time in the presence of stronger speed fluctuations. The kurtosis of displacement can be measured directly in video microscopy experiments involving active Brownian particles. The amount of positive kurtosis at short times will show the importance of speed fluctuations in their dynamics.

V. DISPLACEMENT DISTRIBUTIONS

To gain further insights into the dynamical crossovers, we present displacement distributions obtained from direct numerical simulations for ABP trajectories of dimensionless length $\tilde{L} = L/\bar{\ell}$ with $L = v_0 t$ at a fixed activity $\text{Pe} = v_0 \tau_r/\bar{\ell} = 31.6$. In Fig. 6, we plot the distribution functions $p(\tilde{r})$ of the scaled displacement $\tilde{r} = r/L$ corresponding to $\tilde{D}_v = D_v \tau_r/\bar{\ell}^2 = 10$ (red solid lines). To clearly identify the impact of speed fluctuations on these distributions, we compare them with distributions obtained for ABPs in the absence of speed fluctuations $\tilde{D}_v = 0$ (green dashed line). They show two kinds of reentrant transitions.

In the presence of speed fluctuations. With increasing length of trajectories the distribution shows a reentrant transition from *compact trajectories* characterized by a unimodal distribution with maximum at $\tilde{r} = 0$ in Fig. 6(a) to one with the maximum corresponding to *extended trajectories* with $\tilde{r} \approx 1$ in Fig. 6(d) to finally return to *compact trajectories* characterized by a Gaussian distribution with the maximum at $\tilde{r} = 0$ in Fig. 6(f). Both the transitions between extended and compact trajectories are mediated by bimodal distributions as

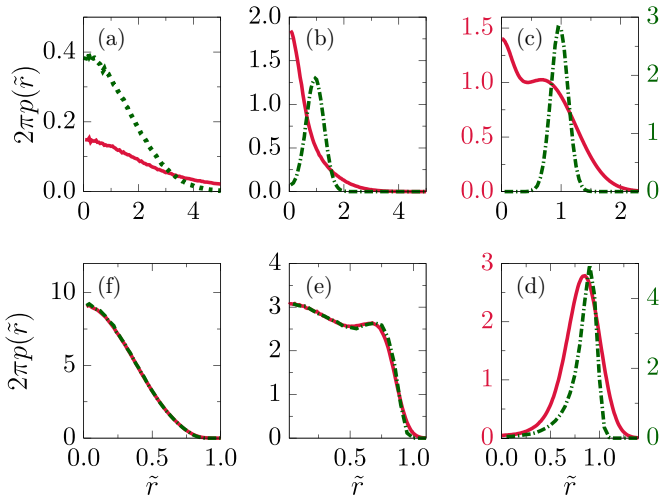


FIG. 6. Probability distributions of displacement $2\pi p(\tilde{r})$ with $\tilde{r} = r/L$ at $\text{Pe} = v_0\tau_r/\bar{\ell} = 31.6$ and $\tilde{D}_v = D_v\tau_r/\bar{\ell}^2 = 10$ (solid line) compared against the results for ABP with constant speed $\tilde{D}_v = 0$ (dashed line) over different time segments $\tilde{L} = v_0t/\bar{\ell} = 0.032$ (a), 0.63 (b), 3.16 (c), 31.62 (d), 126.49 (e), and 316.23 (f). The left (right) $2\pi p(\tilde{r})$ range in (c) and (d) corresponds to $\tilde{D}_v = 10$ ($\tilde{D}_v = 0$ dashed).

can be seen in Figs. 6(c) and 6(e). Such intermediate bimodal distributions describe coexistence of compact and extended trajectories characterizing two *first order* like transitions.

In the absence of speed fluctuations. As is demonstrated in Fig. 6, the displacement distributions at $\tilde{D}_v = 0$ (dashed green lines) show a different kind of reentrant evolution. The initial Gaussian distribution peaked at $\tilde{r} = 0$ characterizing *compact trajectories* [Fig. 6(a)] transits to a distribution with a single maximum near $\tilde{r} = 1$ corresponding to *extended trajectories* [Figs. 6(c) and 6(d)] like ABPs with speed fluctuation. The significant qualitative difference is in the way this transition progresses. It is *continuous* with intermediate distributions being unimodal unlike with $\tilde{D}_v \neq 0$, where the transition is mediated by bimodal distributions. However, at later times the difference between the two cases disappears. The intermediate time unimodal distribution of *extended trajectories* [Fig. 6(d)] returns to a final Gaussian distribution of *compact trajectories* [Fig. 6(f)] via a bimodality in the distribution [Fig. 6(e)] identical to ABPs with speed fluctuations. Thus the reentrant transitions in this case are different—the first *compact-extended* transition is continuous followed by a first order transition between *extended-compact* mediated by their coexistence.

Note that the control parameters \tilde{D}_v and Pe can be expressed in terms of D , $D_p = v_0^2/D_r$, and D_v , the three terms controlling the effective diffusion in Eq. (9), such that $\tilde{D}_v = D_v/D$ and $\text{Pe}^2 = D_p/D$. Thus the relative strength of Pe and $\tilde{D}_v^{1/2}$ influences the displacement statistics. Further, the ratio \tilde{L}/Pe is equivalent to the persistence ratio L/λ of the trajectory length $L = v_0t$ and the persistence length $\lambda = v_0\tau_r$. This ratio is known to control the extension statistics of persistent random walks and wormlike chains [21,55]. As can be seen from Fig. 6, the value of dimensionless trajectory length \tilde{L}

compared to the speed fluctuation scale $\tilde{D}_v^{1/2}$ and the activity Pe determines the properties of the displacement distributions.

In Fig. 6(a) and Fig. 6(b), $\tilde{L} \ll \tilde{D}_v^{1/2} < \text{Pe}$ for $\tilde{D}_v = 10$. From the perspective of directional persistence, the trajectories in this regime are equivalent to rigid rods, as the persistence ratio $\tilde{L}/\text{Pe} = L/\lambda \sim 10^{-2}$. The unimodal distribution $p(\tilde{r})$ with the maximum at $\tilde{r} = 0$ for these quasi-one-dimensional trajectories are determined by the speed fluctuation \tilde{D}_v and translational diffusion D . The increased fluctuation due to \tilde{D}_v in Fig. 6(b) shrinks the trajectories further producing a narrower distribution $p(\tilde{r})$, a behavior absent from trajectories with $\tilde{D}_v = 0$. This behavior changes into a bimodal distribution in Fig. 6(c), where $\tilde{L} \sim \tilde{D}_v^{1/2} < \text{Pe}$. The maximum at the origin is again due to the speed fluctuations. However, compared to the trajectory length, the speed fluctuation is significantly smaller than in the previous two cases, allowing the system to show the second maximum in $p(\tilde{r})$ near $\tilde{r} \approx 1$ corresponding to extended trajectories of persistent motion at $\tilde{L}/\text{Pe} = 0.1$. Note that, for trajectories in the absence of speed fluctuations $\tilde{D}_v = 0$, the maximum at $\tilde{r} = 0$ is absent and, as a result, the distribution remains unimodal with a maximum near $\tilde{r} = 1$. For longer trajectories in Figs. 6(d)–6(f), $\tilde{L} > \tilde{D}_v^{1/2}$, the speed fluctuation can be neglected and the change in $p(\tilde{r})$ is equivalent to ABPs in the absence of speed fluctuations. The transition in this regime can be interpreted in terms of simple persistent motion and equivalently to the WLC polymer [21,55]. The single maximum in $p(\tilde{r})$ in Fig. 6(d) corresponds to extended configurations of a WLC polymer at persistent ratio $\tilde{L}/\text{Pe} = 1$. Similar behavior was observed earlier in Refs. [21,55]. Figure 6(e) corresponds to the persistent ratio $\tilde{L}/\text{Pe} = 4$. The bistability observed in this regime is equivalent to the rigid rod–flexible chain bistability observed for WLCs in the same regime of persistent ratio [55]. For longer trajectories with $\tilde{L}/\text{Pe} = 10$, the distribution turns into unimodal Gaussian distribution with the maximum at $\tilde{r} = 0$. This is the asymptotic long-time behavior of the trajectories and corresponds to the flexible chain limit of WLCs [55].

Note that the first crossover from compact trajectories in Fig. 6(a) to extended trajectories in Fig. 6(d) via the bimodality in Fig. 6(c) is due to the active speed fluctuation. This behavior is absent in ABPs moving with constant speed. The second crossover from the extended state in Fig. 6(d) to the Gaussian compact state in Fig. 6(f) is controlled by persistence as the impact of speed fluctuations for these long trajectories can be neglected. Thus a direct measurement of the displacement distributions can identify the importance of speed fluctuation in the dynamics of active particles. In a recent publication we have shown a mapping of trajectories of ABPs with constant speed and in the presence of thermal diffusion to configurations of a semiflexible polymer [21]. Thus the second crossover seen in the present context is similar to the transition in polymer properties in the WLC model via phase coexistence. The results obtained here map directly to anisotropic ABPs [28,29] interpreting $D_v = D^{\parallel} - D^{\perp}$, where $D^{\perp} = D$.

VI. DISCUSSION

We considered the impact of active speed fluctuations on the d -dimensional motion of an active Brownian particle

(ABP). In the absence of any explicit relaxation mechanism, the model we considered is simpler than, e.g., the Schienbein-Guler model [50,51]. However, it still shows significant departures from ABPs with constant active speed. The speed fluctuation leads to an anisotropy to displacement fluctuations [28,29]. We utilized a Laplace transform method for the Fokker-Planck equation, originally proposed to understand the wormlike chain (WLC) model of semiflexible polymers [46], to find exact expressions for dynamical moments of ABPs in arbitrary dimensions. This method allowed us to obtain several such moments, including the mean-squared displacement, displacement fluctuations parallel and perpendicular to the initial heading direction, and the fourth moment of displacement to characterize the dynamics. Our results showed good agreement with direct numerical simulations. We found several dynamical crossovers and identified the crossover times using the exact analytic expressions. They depend on the activity, persistence, and speed fluctuation of the ABP.

The speed fluctuation in the presence of persistence led to a significant anisotropy. At strong speed fluctuation, the parallel component of displacement fluctuation showed subdiffusive scaling and nonmonotonic variations at intermediate times, unlike the perpendicular component. The exact calculation of kurtosis measuring the non-Gaussian nature of the stochastic displacement remained positive at short times controlled by the speed fluctuation. It crossed over to a negative minimum at intermediate times, a behavior governed by the persistence of motion, before vanishing asymptotically at long times characterizing the asymptotic Gaussian nature of the ABP trajectories.

To further analyze the dynamics, we used direct numerical simulations in two dimensions to obtain the probability distributions of ABP displacement as the time elapsed. It showed reentrant transition with two crossovers between compact and extended trajectories via two separate bimodal distributions at intervening times. The bimodalities signify the coexistence of the compact and extended trajectories. The short-time coexistence is determined by the speed fluctuation and is absent in ABPs with constant speed, as we have shown explicitly. The second coexistence is controlled by persistence and is equivalent to the transition between the rigid rod and flexible polymer via the coexistence of the two conformational phases observed with a change in persistence ratio in the WLC model [55].

The generation of active speed from underlying stochastic mechanisms, e.g., as considered in Refs. [2,40,43,50], involves inherent speed fluctuations. Such fluctuations are present in active colloids performing phoretic motion [9] and mechanisms generating motion in motile cells and bacteria [8,36,37]. Our predictions can be tested in experiments on tagged active particles and our results can be used in analyzing the dynamics of motile cells.

In experiments on active Brownian particles, the impact of speed fluctuations can be most easily observed in the subdiffusive scaling of the parallel component of displacement fluctuation, positive kurtosis, and the evolution of displacement distribution that according to our prediction should show two bimodalities in a reentrant transition from compact to extended to compact trajectories. As we mentioned, speed

fluctuations lead to anisotropy, however, it has a qualitative difference compared to shape anisotropy considered before [28,29]. The shape anisotropy is directly observable in optical microscopy and can be independent of the amount of activity. In contrast, speed anisotropy is expected to increase with activity and is not related to particle shape. This aspect can be directly verified in experiments on active particles.

Note that speed fluctuations can also arise due to interparticle collisions in a dense dispersion of ABPs [33,34]. In their run and tumble motion, several bacteria show switching between different active speeds [38,39]. Our methods can be extended to better understand the nonequilibrium dynamics of such systems.

ACKNOWLEDGMENTS

The numerical calculations were supported in part by SAMKHYA, the high-performance computing facility at the Institute of Physics, Bhubaneswar. We thank A. Dhar for discussions on a related project. D.C. thanks SERB, India for financial support through Grant No. MTR/2019/000750 and International Centre for Theoretical Sciences (ICTS) for an associateship.

APPENDIX A: COMPONENTS OF DISPLACEMENT FLUCTUATION

We assume the initial heading direction $\hat{\mathbf{u}}_0 = \hat{x}$ towards the positive x axis. Thus the second moment of the component of displacement parallel to initial heading direction $r_{\parallel}^2 = x^2$ can be calculated using $\psi = x^2$ in Eq. (5). This gives

$$s\langle r_{\parallel}^2 \rangle_s = 2D_v \langle u_x^2 \rangle_s + 2D/s + 2v_0 \langle xu_x \rangle_s.$$

Using Eq. (5) it is straightforward to show $\langle u_x^2 \rangle_s = \frac{(s+2D_r)}{s(s+2dD_r)}$ and $\langle xu_x \rangle_s = \frac{v_0}{s+(d-1)D_r} \langle u_x^2 \rangle_s$. Thus we obtain

$$\begin{aligned} \langle r_{\parallel}^2 \rangle_s &= \frac{2D_v(s+2D_r)}{s^2(s+2dD_r)} + \frac{2D}{s^2} \\ &+ \frac{2v_0^2(s+2D_r)}{s^2[s+(d-1)D_r](s+2dD_r)}. \end{aligned} \quad (\text{A1})$$

Performing the inverse Laplace transform we find the time dependence,

$$\begin{aligned} \langle r_{\parallel}^2 \rangle &= 2 \left(D + \frac{D_v}{d} + \frac{v_0^2}{(d-1)dD_r} \right) t \\ &+ \frac{(d-1)D_v}{d^2D_r} (1 - e^{-2dD_r t}) \\ &+ \frac{v_0^2}{D_r^2} \left(\frac{(d-1)e^{-2dD_r t}}{d^2(d+1)} + \frac{2(3-d)e^{-(d-1)D_r t}}{(d-1)^2(d+1)} \right. \\ &\left. + \frac{d^2 - 4d + 1}{(d-1)^2 d^2} \right). \end{aligned} \quad (\text{A2})$$

It is easy to obtain the relative fluctuation $\langle \delta r_{\parallel}^2 \rangle = \langle r_{\parallel}^2 \rangle - \langle r_{\parallel} \rangle^2$ noting that the displacement $\langle r_{\parallel} \rangle = \langle \mathbf{r} \cdot \hat{\mathbf{u}}_0 \rangle = \frac{v_0}{(d-1)D_r} (1 - e^{-(d-1)D_r t})$. The fluctuation in the perpendicular component $\langle \delta \mathbf{r}_{\perp}^2 \rangle = \langle \mathbf{r}_{\perp}^2 \rangle$, as the mean $\langle \mathbf{r}_{\perp} \rangle = 0$. Thus $\langle \delta \mathbf{r}_{\perp}^2 \rangle = \langle \mathbf{r}^2 \rangle - \langle r_{\parallel}^2 \rangle$.

APPENDIX B: QUARTIC MOMENT OF DISPLACEMENT

Proceeding as before, using $\psi = \mathbf{r}^4$ in Eq. (5) and the relations

$$\begin{aligned} s\langle \mathbf{r}^4 \rangle_s &= 4D_v[\langle \mathbf{r}^2 \rangle_s + 2\langle (\hat{\mathbf{u}} \cdot \mathbf{r})^2 \rangle_s] + 4(d+2)D\langle \mathbf{r}^2 \rangle_s \\ &\quad + 4v_0\langle (\hat{\mathbf{u}} \cdot \mathbf{r})\mathbf{r}^2 \rangle_s, \\ s\langle \hat{\mathbf{u}} \cdot \mathbf{r} \rangle_s &= -(d-1)D_r\langle \hat{\mathbf{u}} \cdot \mathbf{r} \rangle_s + v_0\langle 1 \rangle_s, \\ s\langle (\hat{\mathbf{u}} \cdot \mathbf{r})^2 \rangle_s &= 2D_v\langle 1 \rangle_s + 2D_r\langle \mathbf{r}^2 \rangle_s - 2dD_r\langle (\hat{\mathbf{u}} \cdot \mathbf{r}) \rangle_s \\ &\quad + 2D\langle 1 \rangle_s + 2v_0\langle \hat{\mathbf{u}} \cdot \mathbf{r} \rangle_s, \\ s\langle (\hat{\mathbf{u}} \cdot \mathbf{r})\mathbf{r}^2 \rangle_s &= 6D_v\langle \hat{\mathbf{u}} \cdot \mathbf{r} \rangle_s - (d-1)D_r\langle (\hat{\mathbf{u}} \cdot \mathbf{r})\mathbf{r}^2 \rangle_s \\ &\quad + (4+2d)D\langle \hat{\mathbf{u}} \cdot \mathbf{r} \rangle_s + v_0\langle \mathbf{r}^2 \rangle_s + 2v_0\langle (\hat{\mathbf{u}} \cdot \mathbf{r})\mathbf{r}^2 \rangle_s, \end{aligned}$$

it is straightforward to obtain the fourth moment of displacement in the Laplace space

$$\begin{aligned} \langle \mathbf{r}^4 \rangle_s &= 8[D_v + (d+2)D](D_v + dD)\frac{1}{s^3} + \frac{16D_v(D_v + D)}{s^2(s + 2dD_r)} \\ &\quad + \frac{32D_v(D_v + D)D_r}{s^3(s + 2dD_r)} + \frac{8D_vv_0^2[5s + 2(d-1)D_r]}{s^3[s + (d-1)D_r]^2} \\ &\quad + \frac{32D_vv_0^2(s + 2D_r)}{s^3[s + (d-1)D_r](s + 2dD_r)} \\ &\quad + \frac{8Dv_0^2(d+2)[3s + 2(d-1)D_r]}{s^3[s + (d-1)D_r]^2} \\ &\quad + \frac{8v_0^4[3s + 2(d+2)D_r]}{s^3[s + (d-1)D_r]^2(s + 2dD_r)}. \end{aligned} \quad (\text{B1})$$

Performing the inverse Laplace transform, one gets the time evolution of the fourth moment.

APPENDIX C: COMPONENTS OF $\langle \delta \mathbf{r}^2 \rangle$ IN THE WEAK SPEED FLUCTUATION ($v_0^2 > D_v D_r$) LIMIT: CROSSOVER ANALYSIS

The parallel component $\langle \delta r_{\parallel}^2 \rangle$ first crosses over from $\langle \delta r_{\parallel}^2 \rangle \sim t$ to $\langle \delta r_{\parallel}^2 \rangle \sim t^3$ at $t_I \approx [3(1 + D/D_v)/4]^{1/2} D_r^{-1}$ followed by another crossover from $\langle \delta r_{\parallel}^2 \rangle \sim t^3$ to $\langle \delta r_{\parallel}^2 \rangle \sim t^4$ at $t_{II} \approx [8D_v D_r / (v_0^2 - 8D_v D_r)] D_r^{-1}$ and finally in the

long time limit a further crossover to $\langle \delta r_{\parallel}^2 \rangle \sim t$ at $t_{III} \approx [5(v_0^2 - 8D_v D_r) / (7v_0^2 - 32D_v D_r)] D_r^{-1}$ when $t_I < t_{II} < t_{III}$ is satisfied. As before, the crossover times are calculated by comparing different terms in Eq. (13). The condition $t_{III} > t_{II}$ leads to $v_0^2 > [(68 + \sqrt{1744})/5] D_v D_r$ and the condition $t_{II} > t_I$ amounts to $v_0^2 < \{16[D_v^3/3(D + D_v)]^{1/2} + 8D_v\} D_r$. Even for $D = 0$, the condition $t_{II} > t_I$ corresponding to $v_0^2 < (16/\sqrt{3} + 8) D_v D_r$ conflicts with the assumption of $v_0^2 > D_v D_r$. It suggests that $\langle \delta r_{\parallel}^2 \rangle \sim t^3$ is not possible. Thus the possible crossovers are $\langle \delta r_{\parallel}^2 \rangle \sim t$ to $\langle \delta r_{\parallel}^2 \rangle \sim t^4$ and finally to $\langle \delta r_{\parallel}^2 \rangle \sim t$. The first crossover $\langle \delta r_{\parallel}^2 \rangle \sim t$ to $\langle \delta r_{\parallel}^2 \rangle \sim t^4$ can appear at

$$t_I^{\parallel} = [6(D + D_v) / (v_0^2 - 8D_v D_r)]^{1/3}$$

and the second crossover $\langle \delta r_{\parallel}^2 \rangle \sim t^4$ to $\langle \delta r_{\parallel}^2 \rangle \sim t$ can appear at

$$t_{II}^{\parallel} = t_{III}^{\parallel} = [5(v_0^2 - 8D_v D_r) / (7v_0^2 - 32D_v D_r)] D_r^{-1}.$$

One possible scenario of crossovers in $\langle \delta \mathbf{r}_{\perp}^2 \rangle$ is the following: (i) from $\langle \delta \mathbf{r}_{\perp}^2 \rangle \sim t$ to $\langle \delta \mathbf{r}_{\perp}^2 \rangle \sim t^3$ at

$$t_I^{\perp} D_r = [3DD_r / (v_0^2 - 4D_v D_r)]^{1/2}$$

with the condition $v_0^2 > 4D_v D_r + 3D_v^2 D_r / D$ ($t_I^{\perp} < t_I^{\parallel}$); (ii) back to $\langle \delta \mathbf{r}_{\perp}^2 \rangle \sim t$ at

$$t_{III}^{\perp} D_r = [4(v_0^2 - 4D_v D_r) / (5v_0^2 - 16D_v D_r)]$$

if the condition $v_0^2 > [(47 + \sqrt{417})/8] D_v D_r$ ($t_{III}^{\perp} < t_{III}^{\parallel}$) is satisfied. Moreover, $t_{III} > t_I$ leads to the condition $v_0^2 > 16(D - D_v) D_v D_r / (5D - 4D_v)$.

Another scenario of possible crossovers are $\langle \delta \mathbf{r}_{\perp}^2 \rangle \sim t$ to $\langle \delta \mathbf{r}_{\perp}^2 \rangle \sim t^2$ at

$$t_I^{\perp} D_r = D / D_v$$

with condition $v_0^2 < 4D_v D_r + 3D_v^2 D_r / D$ ($t_I^{\perp} > t_I^{\parallel}$) to $\langle \delta \mathbf{r}_{\perp}^2 \rangle \sim t^3$ at

$$t_{II}^{\perp} = 3D_v / (v_0^2 - 4D_v D_r)$$

with condition $v_0^2 > [(47 + \sqrt{417})/8] D_v D_r$ ($t_{II}^{\perp} > t_{II}^{\parallel}$) to $\langle \delta \mathbf{r}_{\perp}^2 \rangle \sim t$ with condition $v_0^2 > 4D_v D_r$ at $t_{III}^{\perp} D_r$.

[1] T. Vicsek and A. Zafeiris, *Phys. Rep.* **517**, 71 (2012).
[2] P. Romanczuk, M. Bär, W. Ebeling, B. Lindner, and L. Schimansky-Geier, *Eur. Phys. J.: Spec. Top.* **202**, 1 (2012).
[3] R. D. Astumian and P. Hänggi, *Phys. Today* **55**(11), 33 (2002).
[4] P. Reimann, *Phys. Rep.* **361**, 57 (2002).
[5] H. C. Berg and D. A. Brown, *Nature (London)* **239**, 500 (1972).
[6] H. S. Niwa, *J. Theor. Biol.* **171**, 123 (1994).
[7] F. Ginelli, F. Peruani, M.-H. Pillot, H. Chaté, G. Theraulaz, and R. Bon, *Proc. Natl. Acad. Sci. USA* **112**, 12729 (2015).
[8] M. C. Marchetti, J. F. Joanny, S. Ramaswamy, T. B. Liverpool, J. Prost, M. Rao, and R. A. Simha, *Rev. Mod. Phys.* **85**, 1143 (2013).
[9] C. Bechinger, R. Di Leonardo, H. Löwen, C. Reichhardt, G. Volpe, and G. Volpe, *Rev. Mod. Phys.* **88**, 045006 (2016).

[10] M. Bär, R. Großmann, S. Heidenreich, and F. Peruani, *Annu. Rev. Condens. Matter Phys.* **11**, 441 (2020).
[11] S. Das, G. Gompper, and R. G. Winkler, *New J. Phys.* **20**, 015001 (2018).
[12] C. Kurzthaler, C. Devailly, J. Arlt, T. Franosch, W. C. K. Poon, V. A. Martinez, and A. T. Brown, *Phys. Rev. Lett.* **121**, 078001 (2018).
[13] K. Malakar, V. Jemseena, A. Kundu, K. Vijay Kumar, S. Sabhapandit, S. N. Majumdar, S. Redner, and A. Dhar, *J. Stat. Mech.: Theory Exp.* (2018) 043215.
[14] U. Basu, S. N. Majumdar, A. Rosso, and G. Schehr, *Phys. Rev. E* **98**, 062121 (2018).
[15] F. Peruani and L. G. Morelli, *Phys. Rev. Lett.* **99**, 010602 (2007).

- [16] U. Basu, S. N. Majumdar, A. Rosso, and G. Schehr, *Phys. Rev. E* **100**, 062116 (2019).
- [17] S. N. Majumdar and B. Meerson, *Phys. Rev. E* **102**, 022113 (2020).
- [18] C. G. Wagner, M. F. Hagan, and A. Baskaran, *J. Stat. Mech.: Theory Exp.* (2017) 043203.
- [19] J. Elgeti, R. G. Winkler, and G. Gompper, *Rep. Prog. Phys.* **78**, 056601 (2015).
- [20] A. Dhar, A. Kundu, S. N. Majumdar, S. Sabhapandit, and G. Schehr, *Phys. Rev. E* **99**, 032132 (2019).
- [21] A. Shee, A. Dhar, and D. Chaudhuri, *Soft Matter* **16**, 4776 (2020).
- [22] I. Santra, U. Basu, and S. Sabhapandit, *Phys. Rev. E* **101**, 062120 (2020).
- [23] I. Santra, U. Basu, and S. Sabhapandit, *Phys. Rev. E* **104**, L012601 (2021).
- [24] I. Santra, U. Basu, and S. Sabhapandit, *Soft Matter* **17**, 10108 (2021).
- [25] A. Pototsky and H. Stark, *Europhys. Lett.* **98**, 50004 (2012).
- [26] K. Malakar, A. Das, A. Kundu, K. V. Kumar, and A. Dhar, *Phys. Rev. E* **101**, 022610 (2020).
- [27] D. Chaudhuri and A. Dhar, *J. Stat. Mech.: Theory Exp.* (2021) 013207.
- [28] C. Kurzthaler, S. Leitmann, and T. Franosch, *Sci. Rep.* **6**, 36702 (2016).
- [29] B. ten Hagen, B. ten Hagen, S. van Teeffelen, and H. Löwen, *J. Phys.: Condens. Matter* **23**, 194119 (2011).
- [30] F. J. Sevilla, *Phys. Rev. E* **101**, 022608 (2020).
- [31] J. R. Howse, R. A. L. Jones, A. J. Ryan, T. Gough, R. Vafabakhsh, and R. Golestanian, *Phys. Rev. Lett.* **99**, 048102 (2007).
- [32] J. Palacci, C. Cottin-Bizonne, C. Ybert, and L. Bocquet, *Phys. Rev. Lett.* **105**, 088304 (2010).
- [33] G. S. Redner, M. F. Hagan, and A. Baskaran, *Phys. Rev. Lett.* **110**, 055701 (2013).
- [34] Y. Fily, A. Baskaran, and M. F. Hagan, *Soft Matter* **10**, 5609 (2014).
- [35] F. J. Sevilla and L. A. Gómez Nava, *Phys. Rev. E* **90**, 022130 (2014).
- [36] Y. Wu, A. D. Kaiser, Y. Jiang, and M. S. Alber, *Proc. Natl. Acad. Sci. USA* **106**, 1222 (2009).
- [37] M. Theves, J. Taktikos, V. Ziburdaev, H. Stark, and C. Beta, *Biophys. J.* **105**, 1915 (2013).
- [38] E. Perez Ipiña, S. Otte, R. Pontier-Bres, D. Czerucka, and F. Peruani, *Nat. Phys.* **15**, 610 (2019).
- [39] S. Otte, E. P. Ipiña, R. Pontier-Bres, D. Czerucka, and F. Peruani, *Nat. Commun.* **12**, 1990 (2021).
- [40] F. Schweitzer, W. Ebeling, and B. Tilch, *Phys. Rev. Lett.* **80**, 5044 (1998).
- [41] L. Prawar Dadhichi, A. Maitra, and S. Ramaswamy, *J. Stat. Mech.: Theory Exp.* (2018) 123201.
- [42] S. Ramaswamy, *J. Stat. Mech.: Theory Exp.* (2017) 054002.
- [43] P. Pietzonka and U. Seifert, *J. Phys. A: Math. Theor.* **51**, 01LT01 (2018).
- [44] P. Pietzonka, É. Fodor, C. Lohrmann, M. E. Cates, and U. Seifert, *Phys. Rev. X* **9**, 041032 (2019).
- [45] P. Pietzonka, K. Kleinbeck, and U. Seifert, *New J. Phys.* **18**, 052001 (2016).
- [46] J. J. Hermans and R. Ullman, *Physica* **18**, 951 (1952).
- [47] K. Itô, in *International Symposium on Mathematical Problems in Theoretical Physics*, edited by H. Araki (Springer-Verlag, Berlin-Heidelberg-New York, 1975), Chap. Stochastic Calculus, pp. 218–223.
- [48] M. van den Berg and J. T. Lewis, *Bull. London Math. Soc.* **17**, 144 (1985).
- [49] A. Mijatović, V. Mramor, and G. U. Bravo, *Stat. Probab. Lett.* **165**, 108836 (2020).
- [50] M. Schienbein and H. Gruler, *Bull. Math. Biol.* **55**, 585 (1993).
- [51] A. Shee and D. Chaudhuri, *J. Stat. Mech.: Theory Exp.* (2022) 013201.
- [52] É. Fodor, C. Nardini, M. E. Cates, J. Tailleur, P. Visco, and F. van Wijland, *Phys. Rev. Lett.* **117**, 038103 (2016).
- [53] D. B. Mayer, E. Sarmiento-Gómez, M. A. Escobedo-Sánchez, J. P. Segovia-Gutiérrez, C. Kurzthaler, S. U. Egelhaaf, and T. Franosch, *Phys. Rev. E* **104**, 014605 (2021).
- [54] C. Kurzthaler and T. Franosch, *Soft Matter* **13**, 6396 (2017).
- [55] A. Dhar and D. Chaudhuri, *Phys. Rev. Lett.* **89**, 065502 (2002).